Mechanisms of site-specific photochemistry following core-shell ionization of chemically inequivalent carbon atoms in acetaldehyde (ethanal)

AIP | The Journal of Chemical Physics

Mechanisms of site-specific photochemistry following core-shell ionization of chemically inequivalent carbon atoms in acetaldehyde (ethanal)

Sergey Zagorodskikh, John H. D. Eland, Vitali Zhaunerchyk, Melanie Mucke, Richard J. Squibb, Per Linusson , and Raimund Feifel

Citation: The Journal of Chemical Physics **145**, 124302 (2016); doi: 10.1063/1.4962823
View online: http://dx.doi.org/10.1063/1.4962823
View Table of Contents: http://scitation.aip.org/content/aip/journal/jcp/145/12?ver=pdfcov
Published by the AIP Publishing

Mechanisms of site-specific photochemistry following core-shell ionization of chemically inequivalent carbon atoms in acetaldehyde (ethanal)

Sergey Zagorodskikh,[1,2] John H. D. Eland,[2,3] Vitali Zhaunerchyk,[1,2] Melanie Mucke,[1] Richard J. Squibb,[1,2] Per Linusson,[4] and Raimund Feifel[1,2,a)]
[1]*Department of Physics and Astronomy, Uppsala University, P.O. Box 516, SE-751 20 Uppsala, Sweden*
[2]*Department of Physics, University of Gothenburg, Origovägen 6B, SE-412 96 Gothenburg, Sweden*
[3]*Department of Chemistry, Physical and Theoretical Chemistry Laboratory, Oxford University, South Parks Road, Oxford OX1 3QZ, United Kingdom*
[4]*Department of Physics, Stockholm University, AlbaNova University Center, SE-106 91 Stockholm, Sweden*

(Received 27 April 2016; accepted 2 September 2016; published online 23 September 2016)

Site-specific fragmentation upon 1s photoionisation of acetaldehyde has been studied using synchrotron radiation and a multi-electron-ion coincidence technique based on a magnetic bottle. Experimental evidence is presented that bond rupture occurs with highest probability in the vicinity of the initial charge localisation and possible mechanisms are discussed. We find that a significant contribution to site-specific photochemistry is made by different fragmentation patterns of individual quantum states populated at identical ionisation energies. *Published by AIP Publishing.* [http://dx.doi.org/10.1063/1.4962823]

I. INTRODUCTION

An X-ray photon can excite or remove a core electron in an atom or molecule, forming a core hole state. Within a few femtoseconds, this core hole is usually filled by an electron from an outer shell leading to the emission of an Auger electron,[1,2] which is a highly dominant process in the case of light atoms.[3] In molecules this frequently results in formation of a repulsive state of an ion, which dissociates on a time-scale of tens to hundreds of femtoseconds.

In molecules, core orbitals are normally localised on a particular atomic constituent,[4] which is the reason why they are often labelled using atomic notations. The localisation of such core holes may affect the fragmentation pattern, a phenomenon which is often referred to as site-specific or site-selective photochemistry. This is of great interest for studies of molecular structure and properties at the atomic level, and may possibly provide a way to control chemical reactions.

The photodissociation process has been widely studied using initial resonant core-electron excitation on atoms of different elements[5–8] in a process sometimes referred to as element-specific photochemistry, and on atoms of the same element but in different chemical environments,[9–12] which is referred to as site-specific photochemistry. The dissociation upon core ionisation is relatively less investigated. There are a number of studies related to the case of distinct elements[13–15] but only a few of them concentrated on the fragmentation from core-ionised chemically non-equivalent atoms of a single element. Fukuzawa *et al.*[16] examined this process in the case of CF_3SF_6, Mocellin *et al.*[17] carried out a study on ozone, and Nagaoka *et al.*[18–20] investigated the dissociation of some trihalosilyltrimethylsilyl-compounds upon core ionisation of the silicon 1s and 2p inner shells. Site-specific photochemistry arising from initial ionisation at the all-important carbon atoms of organic molecules was studied by Itälä *et al.*[21] for the case of pyrimidine and by some of us[22] for the case of ethyl trifluoroacetate.

In general, differences in fragmentation behavior can arise in two ways. If the breakdown pattern depends only on the ions' total internal energy content (as assumed in the statistical theory of mass spectra for a molecule of this size), then differences in mass spectra can be caused by differences in the energy deposition that is by differences in the Auger spectra from vacancies on different atoms, defined by the overlap between the core hole and the valence orbital.[6] As known from the very recently investigated cases of acetone,[22] ethyl trifluoroacetate,[23] and acetaldehyde,[24] the Auger spectra from holes on different C atoms can be significantly different. At the other extreme, if Auger decays from different atoms produce exactly the same total energy distribution in the ions, then differences in ion behavior could still arise if the same amount of energy is deposited in different quantum states (including location) which decay in different ways. Differences in fragmentation can arise if the internal energy is vibrational rather than in electronic form, or if it is in electronic states with different charge distributions.[25,27] Fragmentation differences can also arise from spin-orbit and molecular field splittings, as previously found by the Huttula group.[26] In Auger decay such effects can be seen as the influence of the core hole within its lifetime on the nuclear positions and motion, which affects the dicationic states. Therefore the effect can be expected to be more pronounced for longer lifetimes of the core vacancy. For rather small molecules, both differences in the Auger spectra and in the energy localisation may play a role as we discuss in the present work.

Acetaldehyde is an organic compound with the chemical formula CH_3CHO. It is interesting as a relatively small

a)Electronic mail: raimund.feifel@physics.gu.se

molecule with just two chemically different carbon atoms with known core 1s ionisation energies of 294.45 eV (formylic) and 291.80 eV (methylic), respectively, as well as an oxygen 1s ionisation energy of 538.64 eV.[28] Its photoionisation spectrum has been examined in the valence energy range[29–32] and in the core ionisation range,[28,32] including the study of shake-up processes[32] and Auger decay.[28,33] The energy-selected fragmentation of singly ionised acetaldehyde was studied by Golovin *et al.*,[34] Bombach *et al.*, [35] and Johnson *et al.*[36] Very recently, we have investigated multi-electron emission processes in acetaldehyde[24] with emphasis on double and triple valence ionisation and site-specific single and double Auger decay. We also investigated core-valence double ionisation of acetaldehyde for direct comparison to theoretical modelling.[37]

In the present work, we examine site-specific and element-specific behavior of acetaldehyde upon photoionisation from the 1s orbitals of the two chemically distinct carbon atoms and of the oxygen atom. We seek to distinguish contributions from the different mechanisms of site-specific fragmentation mentioned above.

II. EXPERIMENTAL AND ANALYSIS DETAILS

The experiments were performed utilising a multi-electron-ion coincidence set-up based on a magnetic bottle electron spectrometer[38] and an ion spectrometer, which was described before.[39,40] This technique allows us to examine the correlations of several electrons and ions originating from the same ionisation event, which makes it possible to monitor the effects of initial charge localisation and of the energy deposited in the dicationic state. Briefly, electrons emitted by the target species are guided by a combination of a strong divergent and a weak homogeneous magnetic field[41] through a flight tube towards a ca. 2 m distant multi-channel plate (MCP) detector capable of handling multiple hits. In this version of the multi-particle magnetic bottle coincidence technique, the strong magnetic field is created by a hollow ring magnet and the weak field by a solenoid. Their relative positions are optimised for collection efficiency and energy resolution, but because of the weaker field of the hollow ring magnet in comparison to the magnet used for electron-only detection, the resolving power on the electron side was limited to about $E/\Delta E \approx 20$.

Positively charged ions were extracted in opposite direction to the electrons into an in-line Wiley McLaren time-of-flight spectrometer[42] passing through the hollow ring magnet. This was achieved without distortion of the electron flight path by applying a pulsed extraction voltage for the ions at a delay after ionisation. The delay is typically a few hundred nanoseconds and is chosen to be the shortest possible delay enabling all relevant electrons to leave the source region before the pulse is applied. The resolving power on the ion side was $m/\Delta m \approx 50$. In order to prevent any disturbance on the electron flight paths by the high voltage pulsing, an earthed grid has been placed in between the interaction region and the electron flight tube.

We will refer to the ratio between the number of detected particles and the number of particles created in the interaction region as the collection efficiency. In order to be detected, a particle needs to be correctly directed towards the detector and then produces an electron cascade at the MCP detector. Both factors contribute to the collection efficiency and are not distinguishable. Typical collection efficiencies for the current setup are about 40% for electrons and 10% for ions. The electron collection efficiency is effectively independent of energy in the range used in this work. In contrast, the ion collection efficiency may depend significantly on the m/q of the ions for the experimental conditions chosen. Therefore our ability to compare the intensities associated with different masses is limited. However, ratios between the intensities of identical m/q ions detected in coincidence with different electrons should not be affected by the unknown ion collection efficiency. They could be affected by ion translational energies, if these exceed the value at which ions with transverse initial velocities miss the detector. This would be serious for H^+ ions, but is negligible in our apparatus for the heavier ions studied here, so intensities can be reliably compared with each other.

The experiments were carried out at beam line U49/2 PGM-1 of the storage ring BESSY-II at the Helmholtz Zentrum, Berlin, which was operated in a single bunch mode providing 30 ps long light pulses at a repetition rate of about 1.25 MHz. In order to reduce the X-ray pulse repetition rate to a level adequate for unambiguous time referencing of the present experiment (about 10 kHz), we used a mechanical chopper[43] synchronised to the radio frequency signal of the storage ring. Experimental runs were carried out at the photon energies of 307 eV and 550 eV. The energy resolution of the monochromator was $\Delta E < 300$ meV.

The vapor pressure of acetaldehyde at room temperature is sufficiently high to provide a suitable sample gas pressure in the spectrometer without the need for additional heating. The sample was obtained commercially at a stated purity >99%. We used several freeze-pump-thaw cycles in order to remove dissolved air when connecting the sample to the spectrometer. The purity of the sample was verified by recording conventional photoelectron spectra and ion mass spectra both in the valence and core regions and comparing them to reference spectra known from the literature.[31,32,36]

In order to calibrate the conversion of electron flight times to kinetic energies, the carbon 1s photoelectron lines[44] of CO_2 and of acetaldehyde itself[28] were measured at different photon energies.

The conversion to kinetic energy, E_{kin}, uses

$$E_{kin} = \frac{D^2}{(t - t_0)^2} + E_0, \quad (1)$$

where D (which represents the effective length of the electron trajectory), t_0 and E_0 are the calibration parameters determined by least-square fitting of flight times for known energy values. To allow for the non-linearity of this formula, conversion of flight time spectra to energy spectra with a fixed bin size has been done by redistribution of the intensity information from the time bins, as described before.[24,37]

Mass spectra are presented on the experimental time-of-flight scale. The uncertainties in their integrated peak intensities, used to compile the tables, are calculated as one standard deviation of the Poisson distribution.

III. RESULTS AND DISCUSSION

A. Mass spectra for different initial charge localisations

The main result of core ionisation is Auger decay leading to double ionisation,[3] and we shall see that in acetaldehyde the apparently exclusive consequence of double ionisation is charge separation into pairs of singly ionised fragments. To search for site-specific effects on the ion dissociations of doubly charged acetaldehyde, we nevertheless first examine one-dimensional mass spectra extracted in coincidence with each of the photoelectron lines. These spectra are made up of the ion pairs and because of the limited collection efficiency for ions they have better statistics than the detected pairs themselves. We begin with the mass spectra associated with the two well-separated carbon 1s photoelectron lines, which are shown in Fig. 1. As can be seen, substantial differences are observed, and the ratios between peak intensities of the same mass in different spectra, explained in what follows, are summarised in Table I, where the intensities have been derived by integration of each mass peak.

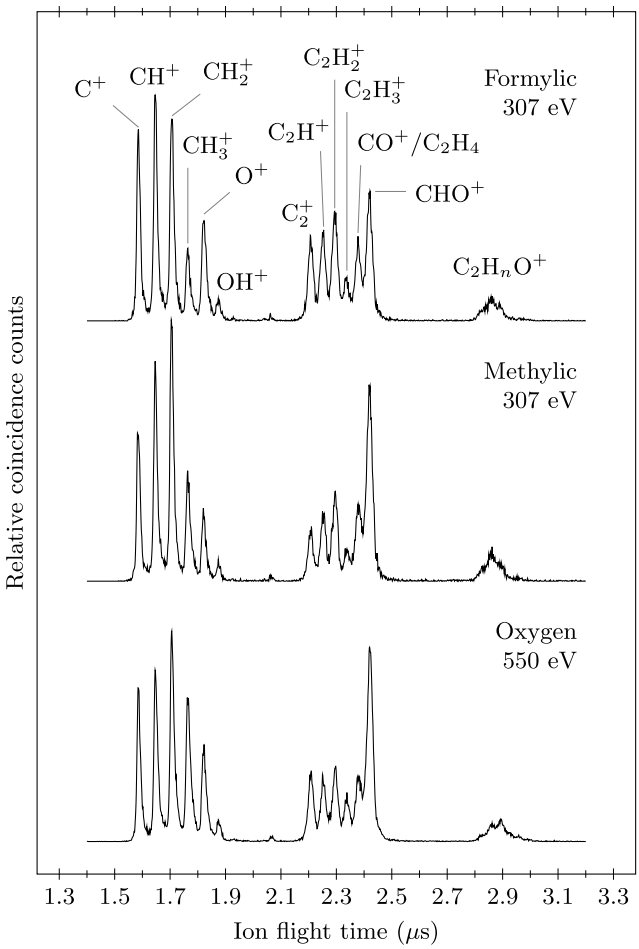

FIG. 1. Mass spectra of acetaldehyde, measured at the photon energies of 307 eV and 550 eV in coincidence with electrons from initial ionisation of the methylic and formylic carbon 1s orbitals as well as the oxygen 1s orbital. Each spectrum is normalised to its total integrated intensity. The bin size is 2 ns.

Each mass spectrum contains three groups of peaks. The group at the longest flight time and weakest in intensity represents the case, where neither the C–O nor C–C bond was broken, but only some of the C–H bonds, leading to the detection of fragments containing all three non-hydrogen atoms of the molecule. The slowest fragment within this group is attributed to mass 44, where the molecular ion has all bonds intact, while the fastest fragment within this group, at mass 40, represents C_2O^+ where the parent molecule has lost all its hydrogen atoms. Due to low intensity and limited instrumental resolution, peaks in this group have a high degree of overlap. In later analysis we will discuss them together as a group, denoted by $C_2H_nO^+$, where $n = 0,1,2,3,4$.

The fragments of the middle group in the spectra shown in Fig. 1 represent cases where either the C–O or the C–C bond is preserved, but not both, giving fragments with two non-hydrogen atoms, varying from mass 24 for C_2^+ to mass 29 for CHO^+ ions.

The third group located in the flight time range of about 1.55–1.9 μs consists of fragments with one non-hydrogen atom as a result of the breakage of either one or both of the C–O and C–C bonds. The fastest fragment in this group is attributed to C^+ with mass 12 and the slowest has mass 17 and is the OH^+ ion, formed by a rearrangement involving hydrogen atom migration.

None of the expected hydrogen-only ions[45] (H^+, H_2^+, and H_3^+) are detected in our present measurements. This is because ion detection has to be inhibited at short flight times in order to avoid interference from breakthrough of the ion extraction pulses. The spectra show no detectable multiply charged ions, although some of the observed fragments are stable in doubly charged form. This indicates that the positive

TABLE I. Formylic carbon to methylic carbon (p_f/p_m) and oxygen to both formylic (p_o/p_f) and methylic (p_o/p_m) carbon ratios between the integrated intensities of peaks discernible in the mass spectra, presented in Fig. 1, of ions detected in coincidence with different core electrons at the photon energies 307 and 550 eV in the case of initial 1s ionisation localised on carbon and oxygen, respectively. The values are multiplied by 100.

m/q	Interpretation	p_f/p_m	p_o/p_f	p_o/p_m
12	C^+	121.8 ± 3.0	81.0 ± 1.7	98.7 ± 2.2
13	CH^+	104.8 ± 2.3	80.2 ± 1.5	84.1 ± 1.6
14	CH_2^+	83.1 ± 1.7	102.3 ± 1.9	85.1 ± 1.5
15	CH_3^+	66.9 ± 2.0	203.2 ± 5.2	135.9 ± 3.1
16	O^+	154.3 ± 4.8	94.2 ± 2.3	145.3 ± 4.1
17	OH^+	132.2 ± 7.9	100.0 ± 4.7	132.2 ± 7.0
24	C_2^+	157.6 ± 5.3	84.7 ± 2.2	133.4 ± 4.1
25	C_2H^+	128.6 ± 3.9	71.3 ± 1.8	91.7 ± 2.6
26	$C_2H_2^+$	126.9 ± 3.5	68.2 ± 1.6	86.5 ± 2.2
27	$C_2H_3^+$	132.6 ± 5.4	100.3 ± 3.2	133.0 ± 4.8
28	$CO^+/C_2H_4^+$	94.1 ± 2.7	92.8 ± 2.4	87.3 ± 2.2
29	CHO^+	64.9 ± 1.5	152.8 ± 3.0	99.2 ± 1.7
40–44	$C_2H_nO^+$	81.1 ± 2.6	109.2 ± 3.1	88.6 ± 2.4

charges in the initial dicationic state always separate before dissociation takes place.

In comparing integrated peak intensities in the mass spectra with initial vacancies on the formylic or methylic carbon atom shown in Fig. 1 and Table I, we see major differences in both the low mass and the intermediate mass groups.

The integrated intensity of the O^+ peak is higher by a factor of approximately 1.54 in the formylic spectrum than in the methylic one. This indicates a higher probability of C–O bond breakage in the case of initial formylic 1s ionisation. Also, the fractions of the $C_2H_n^+$ $(n = 0,1,2,3)$ fragments and the OH^+ fragment are increased by a factor of about 1.27–1.58 in the formylic case, giving additional support for this interpretation. This is a strong indication of a site-specific effect because the C–O bond is next to the formylic carbon atom, but not to the methylic carbon atom. By contrast, the integrated intensities of the fragments CHO^+, CH_3^+, and CH_2^+, which imply breakage of the C–C bond, are larger by factors of about 1.54, 1.50, and 1.20, respectively, when the methylic carbon atom, which is solely adjacent to that bond, is ionised rather than the more distant formylic carbon atom, which is adjacent to both the C–C and the C–O bonds.

Differences in the probability of C–H bond breakage are also apparent. In the methylic spectrum the integrated intensities of the CH_3^+ and CH_2^+ products are higher by factors of about 1.50 and 1.20, respectively. The integral intensity of the C^+ fragment is higher by a factor of 1.22 in the formylic spectrum, while the intensity of CH^+ fragment is about the same in both spectra. Intensities of the CH_3^+ and CH_2^+ to CH^+ and C^+ fragments are difficult to interpret because the first pair can originate only from the methylic group, while the latter two ions may include some contribution from the formylic group. If site-specificity was operative, one might expect bond breakage in the vicinity of the initially ionised core hole, i.e., a more likely detachment of the hydrogen atoms from methylic carbon 1s ionisation. Comparisons between the mass spectra from ionisation at the formylic and methylic carbons do not lead to a clear conclusion on this point, partly because if C–H cleavage occurs, one charge may remain on the hydrogen moiety and so escape detection.

To create a 1s vacancy localised on the oxygen atom we used a photon energy of 550 eV, which is above the oxygen 1s ionisation threshold of acetaldehyde (538.64 eV). The carbon 1s levels are also ionised in this experiment, promoting the ions into the same final states as in the case of the 307 eV measurements, but because we select coincidences with the oxygen 1s photoelectron line, the concurrent carbon 1s ionization does not affect the selected spectrum.

In comparing the mass spectra extracted in coincidence with the oxygen 1s and formylic carbon 1s electrons, one can see that most of the fragments associated with breakage of the C–O bond, namely O^+, C_2^+, C_2H^+, $C_2H_2^+$ are more pronounced in the formylic carbon ionization factors of 1.06, 1.18, 1.40, 1.47, while other two fragments, OH^+ and $C_2H_3^+$ have nearly equal integral intensities in the two mass spectra. This suggests that the C–O bond rupture is more likely if the initial core hole is on the formylic carbon atom than on the oxygen atom. For the fragments associated with the C–C bond dissociation, the oxygen 1s to formylic carbon 1s ratios are about 1.53, 2.03, 1.02 in the cases of CHO^+, CH_3^+, CH_2^+, respectively, which leads to the conclusion that the C–C breaks more easily after ionisation from the oxygen 1s orbital than from the formylic carbon 1s orbital.

Differences between the mass spectra selected in coincidence with the oxygen 1s and methylic carbon 1s ionizations include the products O^+, OH^+, C_2^+, $C_2H_3^+$, whose intensities are enhanced in the oxygen case by factors of about 1.45, 1.32, 1.33, and 1.33, respectively. However, the intensities of the C_2H^+ and $C_2H_2^+$ ions are enhanced in the methylic carbon 1s ionisation by factors of about 1.09 and 1.16, respectively. Since both groups are attributed to the breakage of the C–O bond, this implies that from this comparison it cannot be concluded which of the two 1s ionizations is more likely to break this bond. The fragmentations associated with rupture of the C–C bond also fail to demonstrate a clear trend. CH_3^+ is more pronounced in oxygen 1s ionization (by a factor of about 1.34), but the integral intensity of CH_2^+ is higher (by a factor about 1.18) in the methylic carbon 1s ionization while the probability of detection of CHO^+ is about the same in both cases.

B. Ion pairs measured in coincidence with the oxygen and carbon 1s photoelectrons

As the dominant effect of core ionisation of light atoms is double ionisation by Auger decay leading to fragment ion pair production, a more specific test for site-specificity is to study ion pairs in coincidence with the different 1s lines.

To begin with, the ion pair data are presented as a coincidence map showing the flight time of one of the ion fragments versus another. Fig. 2 illustrates such map in coincidence with the carbon 1s photoelectrons. Events with the flight time difference below 40 ns have been excluded

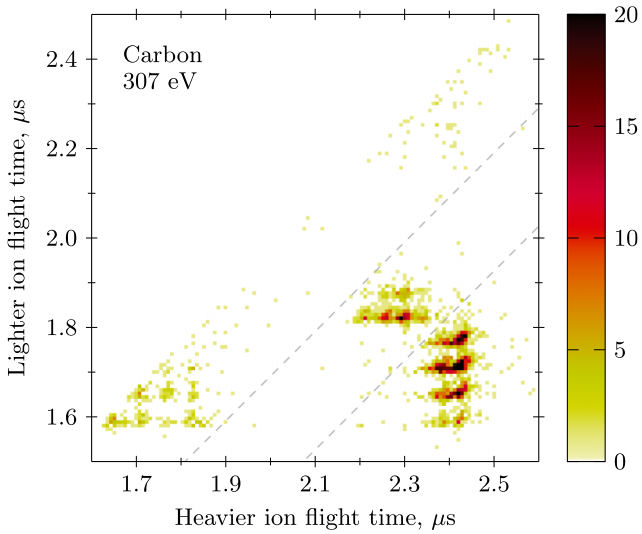

FIG. 2. The ion map of acetaldehyde at the photon energy of 307 eV in coincidence with any of the two carbon 1s photoelectrons. The colour scale represents the number of events within a particular bin. The dotted lines correspond to the flight time difference between ions of 310 and 574 ns. The events with ion flight time difference <40 ns are discarded. The bin size is 8 ns.

to avoid problems of ringing and afterpulsing at the ion detector, but as no abundant fragment pairs of exactly equal mass number are expected[45] this does not constitute a major problem. The flight time range in the map corresponds to the fastest and the middle group of fragments in the mass spectra. The heavy group is not detected in pairs since the only possible partner for the products of this group is hydrogen ions. The limited statistics does not allow us to base an interpretation on the ion production ratios for each individual pair, but the map enables us to discriminate groups of peaks which represent particular bond cleavages. We separate the ion pair products into three groups which are distinct in the map, and can then quantify the integrated intensities of these groups by examining the spectrum of coincident ion arrival time differences, the PIPICO (photoion-photoion coincidence) spectrum.

The identity of the groups in the PIPICO spectrum can be understood as follows: if both the C–C and C–O bonds are broken, the pair with largest possible mass difference is $C^+ + OH^+$, which corresponds to a flight time difference of 285 ns (cf. Fig. 1). Thus, all the pairs corresponding to such dissociation must have this time difference or less. Breaking the C–O bond while leaving the C–C bond intact gives ion pairs such as $C_2^+ + OH^+$ pair and $C_2H_4^+ + O^+$ with time differences between 335 and 558 ns. In dissociation of the C–C bond while retaining the C–O bond the extreme cases are $CH_3^+ + CO^+$ and $C^+ + CHO^+$, which gives time differences in the range of 614 to 831 ns. So these three distinct regions do not overlap and allow us to derive relative probabilities for the breakage of C–C and C–O bonds. In the coincidence map, we have placed the boundaries between these groups at 310 and 574 ns as represented by the grey dashed lines (cf. Fig. 2).

The PIPICO spectra coincident with photoelectrons from the different atoms at the two photon energies are shown in Fig. 3. As can be seen, the coincident PIPICO spectra show rather less marked differences than the simple mass spectra, but

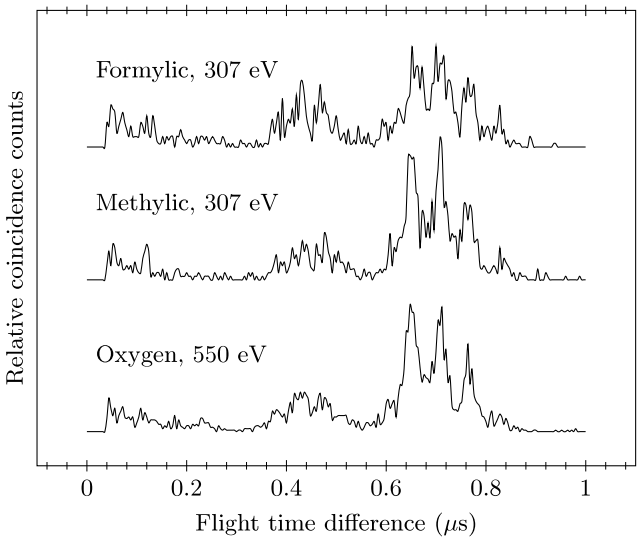

FIG. 3. PIPICO spectra of acetaldehyde, i.e., the difference between ions in each pair selected by electrons associated with the indicated initial core ionisation, at the photon energies of 307 and 550 eV. Each spectrum is independently normalised on its total integrated intensity. The events with ion flight time difference <40 ns are discarded. The bin size is 4 ns.

TABLE II. The integrated intensities of groups of peaks in Fig. 3 in percentage of the total area of a particular spectrum. The "High" group includes peaks above 574 ns difference, the "Low" group corresponds to peaks below 310 ns flight time difference, and the "Mid" group comprises peaks in between.

		307 eV		550 eV
Group	Rupture	Formylic	Methylic	Oxygen
High	C–C	57.1 ± 2.6	68.1 ± 2.9	64.4 ± 1.8
Mid	C–O	26.0 ± 1.5	20.0 ± 1.3	22.6 ± 0.9
Low	Both	16.9 ± 1.2	11.9 ± 1.0	13.0 ± 0.7

the differences are still statistically significant. One important difference between the overall ion spectra and the PIPICO spectra is that hydrogen ions are not detected in either, but any ions created as partners to hydrogen ion species can be detected as ions but not as pairs. Pairs of ions of identical mass (e.g., $CH^+ + CH^+$) are not detected as pairs because of instrumental dead time but could contribute as single ions. Triple ionisation by double Auger decay might also cause the PIPICO and mass spectra to represent different events. This could be significant as we have previously estimated the double to single Auger ratio to be about 29%, 27%, and 21.5% for the oxygen, formylic, and methylic carbon 1s core holes, respectively.[24]

Table II presents a comparison of integrated intensities of the three groups of flight time differences in Fig. 3, corresponding to the breakage of the different bonds. As can be seen from that table, formylic 1s ionisation in comparison to the methylic 1s ionisation leads to a higher probability of breakage of both C–C and C–O bonds and also of breakage of the C–O bond alone. In contrast, in the methylic 1s ionised case, it seems to be more likely to break the C–C only. These trends agree well with the analysis of the mass spectra discussed in Sec. III A.

Comparing initial ionisation at the oxygen site at 550 eV with the carbon sites at 307 eV, we see that the relative integrated intensities of all three groups fall in between the formylic and methylic carbon cases. This is also in agreement with the conclusions made upon comparison of the mass spectra obtained for oxygen and formylic 1s core ionisation. We can conclude that oxygen 1s ionisation is not element-specific, since it provides a lower probability for the breakage of the adjacent C–O bond and a higher probability for the breakage of the distant C–C bond than in the formylic carbon case.

The differences discussed so far amount to about 10% and involve the whole Auger process, that is, the whole range of internal energies deposited in the nascent doubly charged ions. The amount of energy deposited (the magnitude of the energy transfer) can also affect the outcome as seen in acetone.[22]

C. Origin of the site-specific effects

We can now enquire what causes the observed site-specificity, and whether by restricting the energy transfer even more marked site-specific behavior may be revealed. Site-specificity could be caused either by a difference in the energy

deposition (i.e., in the Auger spectra) or by a dependence of the fragmentation from particular energy levels of the doubly charged molecule on the initial charge position. As it is known already for the case of acetaldehyde,[24] there is indeed a substantial difference in the Auger spectra from 1s ionisation at the two carbon atoms. The lowest internal energy states of the doubly ionised products are not significantly populated in formylic Auger decay, while higher internal energy states around 60 eV are populated more strongly.[24]

To examine the effect of internal energy, ideally we should take fourfold coincidence of ion pairs and electron pairs. Unfortunately, the statistics in the present data is too limited for this purpose. Instead, we take ions versus electron pairs, constraining the pairs to contain one selected 1s electron and an Auger electron corresponding to the selected double ionisation energy range. The results for the initial charge formation on two different carbon atoms are shown in Fig. 4. The two maps have been independently normalised to their total integrated intensity in order to eliminate the difference in the initial core hole population. The projections shown above the maps in dots are basically site-specific Auger spectra. We also included the more highly resolved Auger spectra from our previous work.[24] Although such maps contain all the relative intensities, quantitative data are not easy to read from them. To see how the site-specific properties vary with ion internal energies we extract vertical slices of 8 eV width corresponding to different features of the Auger spectra. Their central double ionisation energies are depicted as dotted lines in Fig. 4. The resulting mass spectra are shown in Fig. 5. Each spectrum in this figure has been normalised to its total integrated intensity. The ratios between integrated peak intensities in the formylic and methylic spectra for each slice are summarised in Table III. Due to the limited statistics, we describe here only the most significant differences between each pair of formylic and methylic spectra. At the higher internal energies, above the triple ionisation limit of about 58 eV,[24] any doubly charged state initially populated can autoionise to a triply charged product. The spectra at 62 eV are substantially different from the other three pairs, so there is undoubtedly a triple ionisation contribution in Fig. 5.

The formylic spectrum is dominant in the case of the O^+ fragment at all four double ionisation energies. At 34, 44, and 54 eV the ratio is 1.41, 1.38, and 1.23, respectively, which is lower than for the spectra without energy selection (1.54 times). At 62 eV the ratio is higher, namely 1.87 times. This suggests that the site-specific difference of more probable breakage of the C–O bond upon initial 1s ionisation on the formylic site is less discernible for the narrower band below the triple ionisation threshold (1.41, 1.38, and 1.23 times, respectively), but more significant above the limit (1.87 times).

The main indicator of the C–C bond rupture is the formation of the CHO^+ product, for which the methylic spectrum is dominant in all four selected regions of the internal energy. Similarly to the previous case, the site-specificity at 34, 44, and 54 eV is less pronounced since this peak in the methylic spectra is 1.24, 1.33, and 1.42 times more intense than in the formylic spectra, while in the case of selecting only the 1s electron we had an increase of 1.54. However, the spectra from the states at around 62 eV demonstrate a higher difference by a factor of about 1.81.

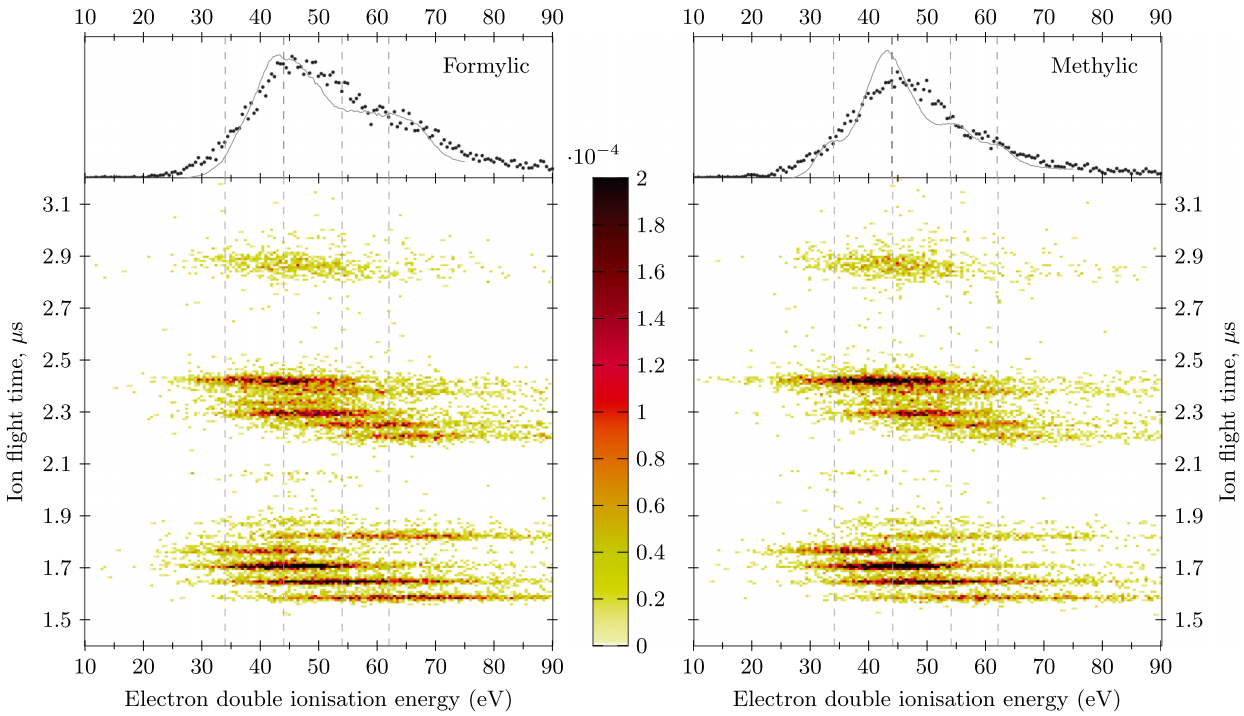

FIG. 4. Coincidence maps of acetaldehyde at the photon energy of 307 eV formed by events with an ion fragment and an Auger electron, selected by either the formylic (left) or methylic (right) 1s core electron. The upper parts represent integrals over the ion flight time in dots. The better resolved Auger spectra adopted from Ref. 24 are shown as solid grey lines. The dashed grey vertical lines show the centers of slices employed to plot the mass spectra in Fig. 5. Each map is independently normalised to its total integrated intensity. The bin size is 0.5 eV × 8 ns.

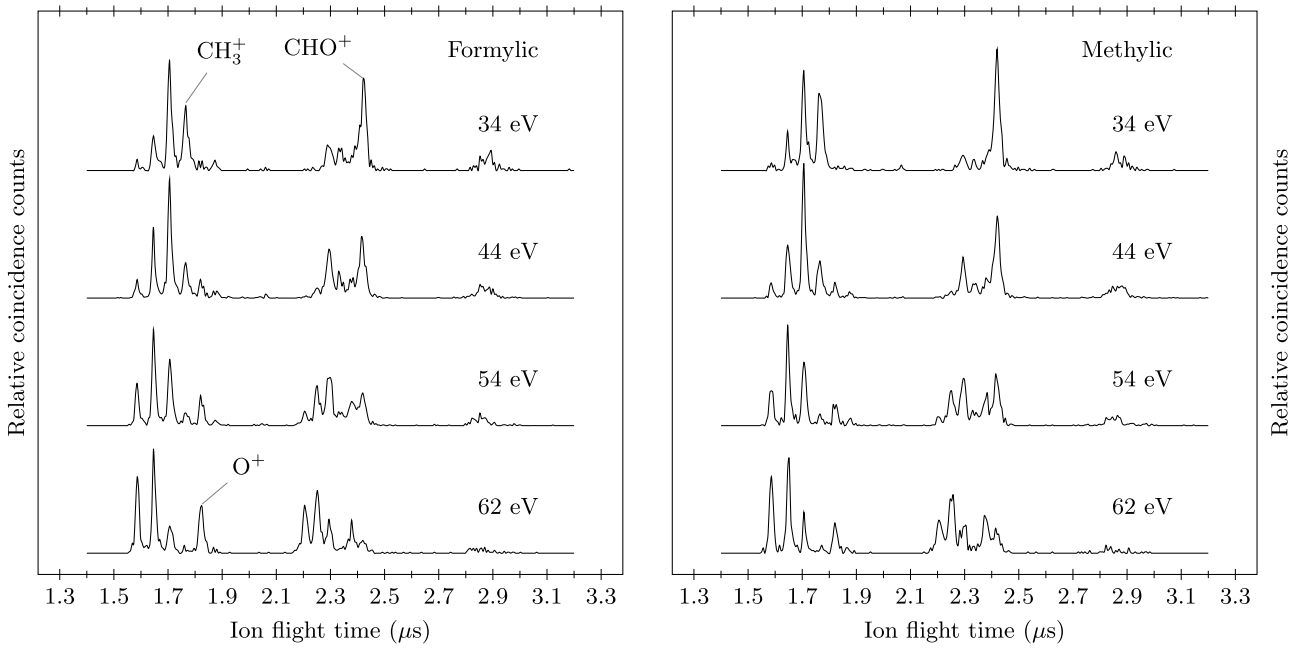

FIG. 5. Mass spectra measured at the photon energy of 307 eV in coincidence with either the formylic (left) or methylic (right) carbon 1s photoelectron and the Auger electron. The curve labels represent the central value of the double ionisation energy. The double ionisation range corresponding to each spectrum is 8 eV, i.e., the central value ±4 eV. The bin size is 8 ns. The full assignment of the peaks is given in Fig. 1.

Regarding the peaks CH_n and C_2H_n ($n = 0,1,2,3$), we note that there is a strong effect of more likely loss of H atoms at higher double ionisation energy. As this effect dominates their intensities, they do not provide signatures for the breakage of the C–O and C–C bonds.

D. The ion yield spectra

Another way of representing the data displayed in the maps of Fig. 4 is to extract horizontal slices among each line corresponding to a particular m/q value, integrate over their width, and plot the integrated intensity of each horizontal slice, i.e., the ion yield as a function of the electron double ionisation energy. The result is called ion yield spectra, which are shown in the bottom panel of Fig. 6 and are grouped in terms of the bond rupture. These spectra can also be understood as site-specific Auger spectra, detected in coincidence with a particular ion in addition to the core photoelectron. The upper panel represents the sum of the spectra in both groups. The products C^+ and CH^+ are included in the group of the C–C break signatures since they definitely require dissociation of this bond. However the fate of the C–O bond is uncertain in their case, since the source of these two products may be either the formylic or the methylic group. We also note that the contribution of different products to the summed spectra may be significantly affected by the collection/detection dependency on m/q.

TABLE III. The formylic to methylic (p_f/p_m) ratios between the integrated intensities of peaks discernible in the mass spectra at the photon energy of 307 eV of ions detected in coincidence with both the core and Auger electrons presented in Fig. 5 multiplied by 100.

m/q	Interpretation	34 eV	44 eV	54 eV	62 eV
12	C^+	95 ± 33	113 ± 17	103 ± 12	96 ± 11
13	CH^+	108 ± 17	94 ± 8	97 ± 8	102 ± 10
14	CH_2^+	102 ± 11	94 ± 6	110 ± 10	98 ± 15
15	CH_3^+	74 ± 8	91 ± 9	122 ± 22	87 ± 28
16	O^+	141 ± 41	138 ± 19	123 ± 17	187 ± 27
17	OH^+	204 ± 75	130 ± 27	77 ± 20	80 ± 31
24	C_2^+	71 ± 62	107 ± 42	133 ± 24	119 ± 15
25	C_2H^+	133 ± 64	160 ± 27	103 ± 11	100 ± 11
26	$C_2H_2^+$	190 ± 35	143 ± 12	114 ± 11	99 ± 15
27	$C_2H_3^+$	283 ± 66	147 ± 18	97 ± 14	57 ± 16
28	$CO^+/C_2H_4^+$	109 ± 20	103 ± 12	92 ± 11	71 ± 10
29	CHO^+	80 ± 8	75 ± 6	70 ± 7	55 ± 10
40–44	$C_2H_nO^+$	108 ± 16	88 ± 9	91 ± 12	117 ± 26

The relative integrated intensities of the summed spectra associated with the C–O breakage in comparison to the spectra associated with the C–C breakage confirm a higher probability of the C–C bond dissociation regardless of the initial charge localisation, as was revealed in the PIPICO spectra displayed in Fig. 3 and summarised in Table II. In addition, the sum of the ion production spectra shows that the C–C bond rupture is most prominent in the case of lower dicationic state energy, roughly below the triple ionisation threshold, while above this threshold the breakage of the C–C and C–O bonds is almost equally probable.

In the case of the summed ion yield spectra associated with the C–O bond rupture, one can see that the formylic spectrum shows higher integrated intensities for all double ionisation energies, but the most significant effect shows up above the maximum located at about 50 eV. These observations suggest again the presence of a site-specific effect reflected in the higher probability of the C–O bond dissociation upon formylic rather than methylic 1s photoionisation.

The sum of the ion yield spectra related to the breakage of the C–C bond shows, however, the opposite behaviour. In this

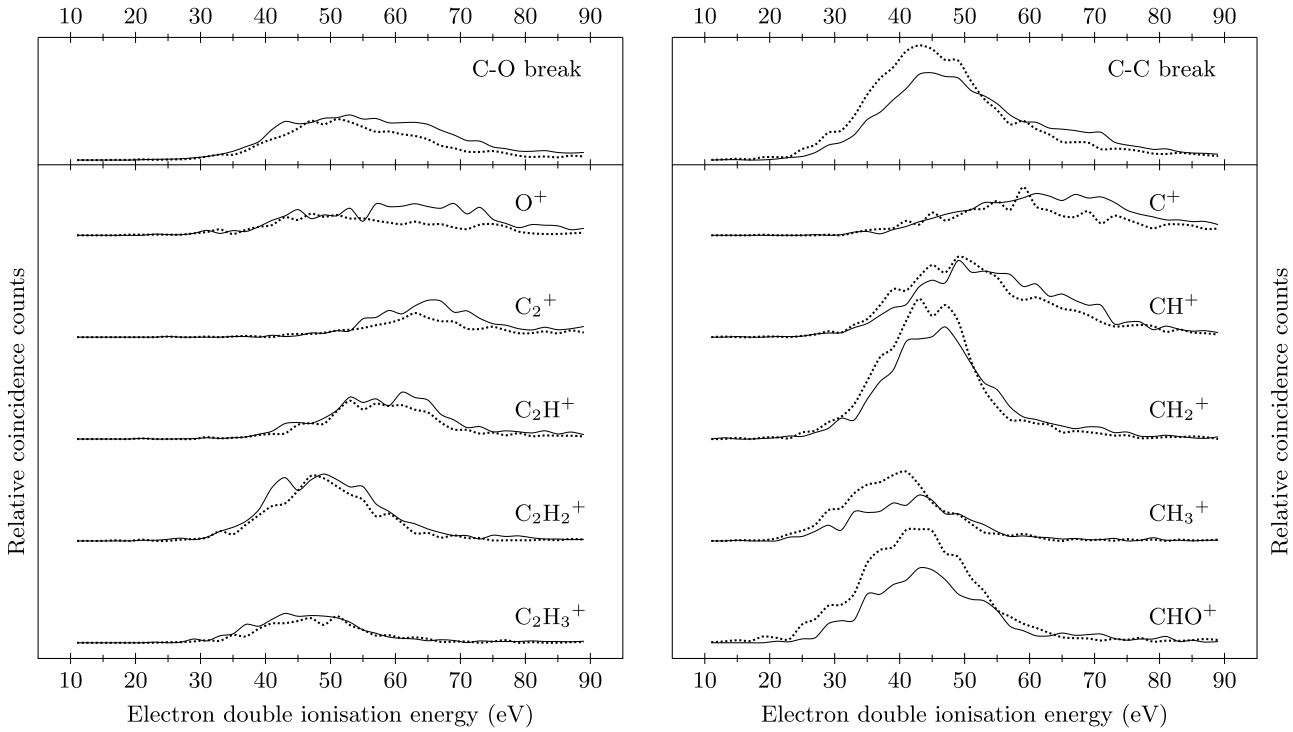

FIG. 6. Bottom panel: Ion yield spectra at the photon energy of 307 eV for different products, detected in coincidence with the formylic (solid line) or methylic (dotted line) carbon 1s photoelectron and an Auger electron corresponding to the double ionisation value displayed on the horizontal axis. The spectra are taken as horizontal slices of the maps in Fig. 4 with no additional normalisation and are grouped by the corresponding bond breakage. In the upper panel the sum of each of the two groups is provided. The bin size is 2 eV.

case the methylic spectrum appears to be more dominant than the formylic spectrum and its maximum prevalence is observed below 50 eV. At the higher double ionisation energy of about 60–75 eV there is a weak dominance of the formylic spectrum, however one can see that the contribution to this part comes mostly from the C^+ and CH^+ products. Thus this observation is likely attributable to a joint C–C and C–O bond rupture.

The pair of spectra selected by the O^+ ion have basically identical character to the C–O breakage spectra, i.e., a relatively broad featureless band where two spectra are very close in intensity in the lower part, but at higher double ionisation energy the dominance of the formylic spectrum is noticeable. This high degree of agreement between two pairs of spectra is expected because the O^+ fragment is generated upon almost every C–O bond dissociation, except for a relatively rare situation, when a rearrangement is engaged resulting in the production of OH^+.

Four pairs of spectra corresponding to the $C_2H_n^+$ ($n = 0,1,2,3$) fragments are very similar to each other in form and width, but the fragments with more hydrogen atoms are found in the lower double ionisation energy range, while the dehydrogenated products lie in somewhat higher energy regions. The shift between these spectra roughly corresponds to the C–H bond dissociation energy, which is a few eV. The formylic spectrum is slightly prevalent for all four products and the formylic-methylic ratios seem to be nearly constant.

In the case of fragments associated with the breakage of the C–C bond, namely CHO^+, CH_3^+, CH_2^+, CH^+, and C^+ for energies below 50–55 eV there is a nearly constant methylic to formylic ratio with a significant dominance of the methylic spectra. Above this value the first three pairs of spectra converge to zero, while in the latter two pairs the formylic spectra become dominant. As was mentioned above, we attribute this to a somewhat higher fraction of CH^+ and C^+ formation originating from a joint rupture of both the C–C and C–O bonds. Akin to the $C_2H_n^+$ ($n = 0,1,2,3$) case, CH_n^+ ($n = 0,1,2,3$) ions are shifted relative to each other by a few eVs due to the C–H bond dissociation energy.

E. The site-specific effect as a function of the dicationic internal energy selection width

In Section III C, we have determined that below the triple ionisation threshold, a comparatively narrow (8 eV) selection on the double ionisation energy as compared with mass spectra not selected on Auger electrons shows less, but still significant difference between the formylic and methylic spectra. In order to understand if the fragmentation behaviour at a particular internal energy can play a role we look at how the difference in mass spectra changes with the width of the internal energy selection. We define the total site-specific difference in the integrated intensities of the mass peaks as

$$P_\Delta = \frac{1}{2}\sum_{i=1}^{N} |p_{fi} - p_{mi}|, \tag{2}$$

where N is the total number of peaks, p_{fi} and p_{mi} are the integrated intensities of the i^{th} peaks of the normalized mass spectrum measured in coincidence with formylic and methylic 1s photoelectrons, respectively, in addition to an Auger electron.

The parameter P_Δ is the characteristic of the degree of difference between two mass spectra. In comparing spectra independently normalised to the total integrated intensity, $P_\Delta = 0\%$ means that the spectra are completely identical (in terms of the integrated peak intensities but not their forms), while $P_\Delta = 100\%$ implies the maximum possible difference, i.e., no common peaks. We are interested in the dependence of the difference between the formylic and methylic spectra as a function of the width of the selected double ionisation energy range defined by the Auger electron kinetic energy. Since P_Δ is defined using the difference between the integrated intensities, it might be affected by the collection efficiency dependence on ion kinetic energy; we assume here that this is not significant.

Fig. 7 shows P_Δ as a function of the selection width. The center of all selections is chosen at the double ionisation energy of 44 eV, roughly corresponding to the maximum of the Auger spectra, which provides optimum statistics for small selection widths and minimises differences due to the energy deposition.

At large widths, where the whole Auger spectrum is included there is a plateau with $P_\Delta \approx 12.6\%$. This is the maximum effect, since all possible mechanisms are involved. With decrease of the selection width, the site-specificity declines as the effects of energy deposition differences and triple ionisation are reduced. If these mechanisms were the only cause of the site-specificity one would expect a decline of P_Δ down to 0%. However, we can see another plateau starting at around 30 eV selection width with $P_\Delta \approx 9.1\%$. Selection width less than 5 eV gives a statistically insignificant result, but extrapolation of the plateau region suggests that P_Δ will stay about the same down to an infinitely small selection width, corresponding to a single dicationic internal energy value. The only localisation effect that remains if the ions have exactly the same amount of internal energy must come from the effect of a particular core hole on the nuclear positions and motion prior to Auger electron emission that is on movement of the nuclei within the few femtoseconds available before Auger decay. Any such nuclear motion will be dependent on the location of the core hole causing the internal energy to be in different internal degrees of freedom.

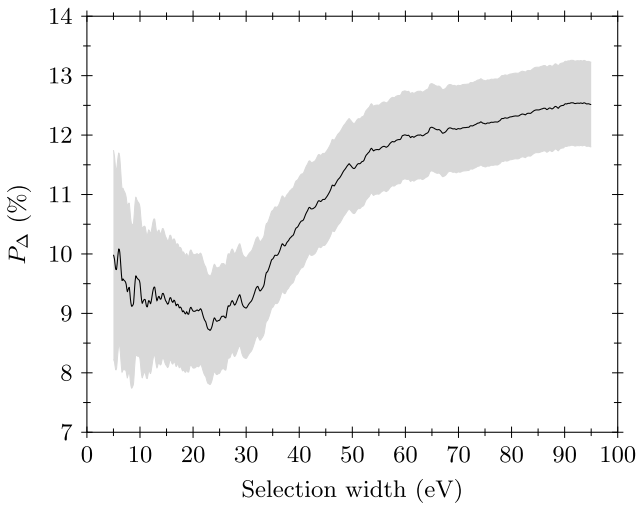

FIG. 7. The total site-specific difference (see Equation (2)) between the integrated intensities of peaks in the mass spectra measured in coincidence with the formylic and methylic 1s electron and an Auger electron at the photon energy of 307 eV as a function of double ionisation energy selection width. The center of the selection is chosen near the maximum of the Auger spectra, i.e., at the double ionisation energy of 44 eV. The grey area represents the statistical uncertainty.

IV. CONCLUSIONS

In mass and ion-ion coincidence spectra of acetaldehyde at a photon energy of 307 eV in coincidence with the chemically different carbon 1s photoelectrons, we have uncovered site-specific effects of the initial charge location. Breakage of the C–C bond is more probable and breakage of the C–O bond is less probable after core ionisation at the methylic carbon atom rather than the formylic one. Breakage of both the C–C and C–O bonds is more likely after formylic carbon ionisation. These and other related site-specific effects may arise in two possible ways: either from the different amounts of energy deposited in the dications by the Auger decays or from different fragmentation behavior of individual quantum states. Individual states with different distributions of the same total internal energy may be populated as a consequence of nuclear motions and electron reorganisation induced by localised core hole creation.

Mass spectra selected for narrow double ionisation energy ranges following ejection of the different core photoelectrons have allowed us to quantify these different contributions.

With the aid of a site-specificity parameter P_Δ defined in this work we have shown that differences in fragmentation behavior between initial ionisations at the formylic and methylic carbon atoms probably persist even for identical internal energy contents in the nascent doubly charged ions, as exemplified for selections of varying widths centered at the double ionisation energy of 44 eV. Such differences represent a true site-specific effect caused by local effects of the initial core hole on the atom positions and energy distributions.

ACKNOWLEDGMENTS

This work has been financially supported by the Swedish Research Council (VR) and the Knut and Alice Wallenberg Foundation, Sweden. We would like to warmly acknowledge the support by the staff and colleagues at the Helmholtz Centre for Materials and Energy GmbH BESSY-II, Berlin. This work was also supported by the European Community — Research Infrastructure Action under the FP6 "Structuring the European Research Area" Programme (through the Integrated Infrastructure Initiative "Integrating Activity on Synchrotron and Free Electron Laser Science." — Contract No. R II 3-CT-2004-506008).

[1]L. Meitner, Z. Phys. **9**, 131 (1922).
[2]P. Auger, J. Phys. Radium **6**, 205 (1925).
[3]R. Santra, J. Phys. B: At., Mol. Opt. **42**, 023001 (2009).
[4]H. Ågren, A. Cesar, and C.-M. Liegener, in *Advances in Quantum Chemistry*, edited by P.-O. Löwdin, J. R. Sabin, and M. C. Zerner (Academic Press, 1992), Vol. 23, pp. 1–82.
[5]R. Murphy and W. Eberhardt, J. Chem. Phys. **89**, 4054 (1988).

[6]C. Miron, M. Simon, N. Leclercq, D. L. Hansen, and P. Morin, Phys. Rev. Lett. **81**, 4104 (1998).
[7]X. J. Liu, G. Prümper, E. Kukk, R. Sankari, M. Hoshino, C. Makochekanwa, M. Kitajima, H. Tanaka, H. Yoshida, Y. Tamenori, and K. Ueda, Phys. Rev. A **72**, 042704 (2005).
[8]P. Salén, M. Kaminska, R. J. Squibb, R. Richter, M. Alagia, S. Stranges, P. van der Meulen, J. H. D. Eland, R. Feifel, and V. Zhaunerchyk, Phys. Chem. Chem. Phys. **16**, 15231 (2014).
[9]W. Eberhardt, T. K. Sham, R. Carr, S. Krummacher, M. Strongin, S. L. Weng, and D. Wesner, Phys. Rev. Lett. **50**, 1038 (1983).
[10]K. Müller-Dethlefs, M. Sander, L. A. Chewter, and E. W. Schlag, J. Phys. Chem. **88**, 6098 (1984).
[11]S.-Y. Chen, C.-I. Ma, D. M. Hanson, K. Lee, and D. Y. Kim, J. Electron Spectrosc. Relat. Phenom. **93**, 61 (1998).
[12]A. Naves de Brito, S. Sundin, R. R. Marinho, I. Hjelte, G. Fraguas, T. Gejo, N. Kosugi, S. Sorensen, and O. Björneholm, Chem. Phys. Lett. **328**, 177 (2000).
[13]K. Le Guen, M. Ahmad, D. Céolin, P. Lablanquie, C. Miron, F. Penent, P. Morin, and M. Simon, J. Chem. Phys. **123**, 084302 (2005).
[14]H. Fukuzawa, G. Prümper, X. J. Liu, E. Kukk, R. Sankari, M. Hoshino, H. Tanaka, Y. Tamenori, and K. Ueda, Chem. Phys. Lett. **436**, 51 (2007).
[15]H. Levola, E. Itälä, K. Schlesier, K. Kooser, S. Laine, J. Laksman, D. T. Ha, E. Rachlew, M. Tarkanovskaja, K. Tanzer, and E. Kukk, Phys. Rev. A **92**, 063409 (2015).
[16]H. Fukuzawa, G. Prümper, S.-i. Nagaoka, T. Ibuki, Y. Tamenori, J. Harries, X. Liu, and K. Ueda, Chem. Phys. Lett. **431**, 253 (2006).
[17]A. Mocellin, K. Wiesner, S. L. Sörensen, C. Miron, K. Le Guen, D. Céolin, M. Simon, P. Morin, A. B. Machado, O. Björneholm, and A. Naves de Brito, Chem. Phys. Lett. **435**, 214 (2007).
[18]S. Nagaoka, Y. Tamenori, M. Hino, T. Kakiuchi, J. Ohshita, K. Okada, T. Ibuki, and I. H. Suzuki, Chem. Phys. Lett. **412**, 459 (2005).
[19]S. Nagaoka, G. Prümper, H. Fukuzawa, M. Hino, M. Takemoto, Y. Tamenori, J. Harries, I. H. Suzuki, O. Takahashi, K. Okada, K. Tabayashi, X.-J. Liu, T. Lischke, and K. Ueda, Phys. Rev. A **75**, 020502 (2007).
[20]S. Nagaoka, H. Fukuzawa, G. Prümper, M. Takemoto, O. Takahashi, K. Yamaguchi, T. Kakiuchi, K. Tabayashi, I. H. Suzuki, J. R. Harries, Y. Tamenori, and K. Ueda, J. Phys. Chem. A **115**, 8822 (2011).
[21]E. Itälä, D. Ha, K. Kooser, M. Huels, E. Rachlew, E. Nõmmiste, U. Joost, and E. Kukk, J. Electron Spectrosc. Relat. Phenom. **184**, 119 (2011).
[22]J. H. D. Eland, P. Linusson, M. Mucke, and R. Feifel, Chem. Phys. Lett. **548**, 90 (2012).
[23]H. Iwayama, N. Sisourat, P. Lablanquie, F. Penent, J. Palaudoux, L. Andric, J. H. D. Eland, K. Bučar, M. Žitnik, Y. Velkov, Y. Hikosaka, M. Nakano, and E. Shigemasa, J. Chem. Phys. **138**, 024306 (2013).
[24]S. Zagorodskikh, V. Zhaunerchyk, M. Mucke, J. H. D. Eland, R. J. Squibb, L. Karlsson, P. Linusson, and R. Feifel, Chem. Phys. **463**, 159 (2015).
[25]J. A. Kettunen, S. Urpelainen, S. Heinäsmäki, and M. Huttula, Phys. Rev. A **86**, 023201 (2012).
[26]E. Kokkonen, T. Löytynoja, K. Jänkälä, J. A. Kettunen, S. Heinäsmäki, A. Karpenko, and M. Huttula, J. Chem. Phys. **140**, 184304 (2014).
[27]E. Kokkonen, T. Löytynoja, L. Hautala, K. Jänkälä, and M. Huttula, J. Chem. Phys. **143**, 074307 (2015).
[28]N. Correia, A. Naves de Brito, M. P. Keane, L. Karlsson, S. Svensson, C.-M. Liegener, A. Cesar, and H. Ågren, J. Chem. Phys. **95**, 5187 (1991).
[29]D. Chadwick and A. Katrib, J. Electron Spectrosc. Relat. Phenom. **3**, 39 (1974).
[30]W.-C. Tam, D. Yee, and C. E. Brion, J. Electron Spectrosc. Relat. Phenom. **4**, 77 (1974).
[31]K. Kimura, S. Katsumata, T. Yamazaki, and H. Wakabayashi, J. Electron Spectrosc. Relat. Phenom. **6**, 41 (1975).
[32]M. P. Keane, S. Lunell, A. Naves de Brito, M. Carlsson-Göthe, S. Svensson, B. Wannberg, and L. Karlsson, J. Electron Spectrosc. Relat. Phenom. **56**, 313 (1991).
[33]D. Minelli, F. Tarantelli, A. Sgamellotti, and L. S. Cederbaum, J. Electron Spectrosc. Relat. Phenom. **74**, 1 (1995).
[34]A. V. Golovin, Y. L. Sergeev, M. E. Akopyan, and F. I. Vilesov, Theor. Exp. Chem. **13**, 580 (1978).
[35]R. Bombach, J.-P. Stadelmann, and J. Vogt, Chem. Phys. **60**, 293 (1981).
[36]K. Johnson, I. Powis, and C. J. Danby, Chem. Phys. **70**, 329 (1982).
[37]S. Zagorodskikh, M. Vapa, O. Vahtras, V. Zhaunerchyk, M. Mucke, J. H. D. Eland, R. J. Squibb, P. Linusson, K. Jänkälä, H. Ågren, and R. Feifel, Phys. Chem. Chem. Phys. **18**, 2535 (2016).
[38]J. H. D. Eland, O. Vieuxmaire, T. Kinugawa, P. Lablanquie, R. I. Hall, and F. Penent, Phys. Rev. Lett. **90**, 053003 (2003).
[39]J. H. D. Eland and R. Feifel, Chem. Phys. **327**, 85 (2006).
[40]R. Feifel, J. H. D. Eland, L. Storchi, and F. Tarantelli, J. Chem. Phys. **125**, 194318 (2006).
[41]P. Kruit and F. H. Read, J. Phys. E: Sci. Instrum. **16**, 313 (1983).
[42]W. C. Wiley and I. H. McLaren, Rev. Sci. Instrum. Instruments **26**, 1150 (1955).
[43]S. Plogmaker, P. Linusson, J. H. D. Eland, N. Baker, E. M. J. Johansson, H. Rensmo, R. Feifel, and H. Siegbahn, Rev. Sci. Instrum. **83**, 013115 (2012).
[44]G. Johansson, J. Hedman, A. Berndtsson, M. Klasson, and R. Nilsson, J. Electron Spectrosc. Relat. Phenom. **2**, 295 (1973).
[45]E. Ruhl, S. Price, S. Leach, and J. H. D. Eland, Int. J. Mass Spectrom. Ion Processes **97**, 175 (1990).